

# Tentative Detection of the Cosmic Infrared Background at 2.2 and 3.5 $\mu\text{m}$ Using Ground Based and Space Based Observations

V. Gorjian

*Jet Propulsion Laboratory, California Institute of Technology, 4800 Oak Grove Dr., Pasadena,  
CA 91109*

`vg@jpl.nasa.gov`

and

E. L. Wright and R. R. Chary

*Department of Physics and Astronomy, University of California, Los Angeles, CA 90095-1562*

`wright@astro.ucla.edu, rchary@astro.ucla.edu`

## ABSTRACT

The Cosmic InfraRed Background (CIRB) is the sum total of the redshifted and reprocessed short wavelength radiation from the era of galaxy formation, and hence contains vital information about the history of galactic evolution. One of the main problems associated with estimating an isotropic CIRB in the near infrared (1-5  $\mu\text{m}$ ) is the unknown contribution from stars within our own galaxy. The optimal observational window to search for a background in the near-IR is at 3.5  $\mu\text{m}$  since that is the wavelength region where the other main foreground, the zodiacal dust emission, is the least. It is not possible to map out the entire 3.5  $\mu\text{m}$  sky at a resolution which will accurately estimate the flux from stars. However, since the CIRB is presumably isotropic, it can potentially be detected by selecting a smaller field and imaging it at good resolution to estimate the stellar intensity. We selected a  $2^\circ \times 2^\circ$  “dark spot” near the North Galactic Pole which had the least intensity at 3.5  $\mu\text{m}$  after a zodiacal light model was subtracted from the all-sky maps generated by the Diffuse InfraRed Background Experiment (DIRBE). Still, the large area of the field made it very difficult to mosaic at 3.5  $\mu\text{m}$  using the available arrays. Thus, the field was mosaiced at 2.2  $\mu\text{m}$ , then the bright stars were selected and re-imaged at 2.2 and 3.5  $\mu\text{m}$ . The resulting total intensity of the bright stars was combined with a model for the contribution from dimmer stars and subtracted from the zodi-subtracted DIRBE map. The contribution from the interstellar medium was also subtracted leaving a residual intensity at 2.2  $\mu\text{m}$  of:  $16.4 \pm 4.4 \text{ kJy sr}^{-1}$  or  $22.4 \pm 6.0 \text{ nW m}^{-2} \text{ sr}^{-1}$ , and at 3.5  $\mu\text{m}$  of:  $12.8 \pm 3.8 \text{ kJy sr}^{-1}$  or  $11.0 \pm 3.3 \text{ nW m}^{-2} \text{ sr}^{-1}$ . The nature of our analysis suggests that this excess emission is probably a detection of the cosmic background in the near infrared.

*Subject headings:* cosmology: observations — diffuse radiation — infrared:general

## 1. Introduction

One of the few tools available for studying the “Dark Ages” following the era of matter-radiation decoupling is the Cosmic InfraRed Background (CIRB) radiation. The CIRB is the result of the cumulative, short wavelength emissions from pregalactic, protogalactic, and galactic systems which through dust reprocessing and cosmological redshifting are now at infrared wavelengths. Although the importance of looking for an extragalactic infrared background has been discussed for some time (Partridge and Peebles 1967; Low and Tucker 1968; Peebles 1969; Harwit 1970; Kaufman 1976), relatively little theoretical attention had been paid to it due to the difficulties inherent in trying to observe and verify theoretical predictions. But advances in infrared technology have stimulated an increasing amount of interest in trying to determine the characteristics of the CIRB (Bond *et al.* 1986; McDowell 1986; Fabbri *et al.* 1987; Fabbri 1988; Bond *et al.* 1991; Lonsdale 1995; Malkan & Stecker 1998; Pei *et al.* 1999). The theoretical work indicates that measuring the spectral intensity and the anisotropy of the CIRB will have important implications regarding the amount of matter undergoing luminous episodes in the pregalactic Universe, the nature and evolution of those luminosity sources, the nature and distribution of cosmic dust, and the density and luminosity evolution of infrared-bright galaxies (for review see Hauser (1996)).

Although technology is no longer a hindrance in observing the CIRB, there are other difficulties in trying to see this cosmic relic. The bright foreground from the atmosphere of the earth, the dust in the solar system, and the stellar and interstellar emissions of our own galaxy combine to make detecting the CIRB a formidable task.

Several experiments have been carried out to try to determine the CIRB from within the atmosphere. Matsumoto *et al.* (1988) and Noda *et al.* (1992) used rocket borne cameras to try to escape the contamination from the atmosphere and observe the CIRB. They had only limited success and could set upper limits on the CIRB without any detections. Lower limits were determined from deep galaxy counts conducted in the near-IR. These two limits began setting the first tight constraints on galaxy evolution models.

The logical next step in trying to detect the CIRB was to go into space to try and eliminate the more local foreground; thus, the Cosmic Background Explorer (COBE) satellite carried with it an experiment specifically designed to detect the CIRB (Boggess *et al.* 1992). The Diffuse InfraRed Background Experiment (DIRBE) was cryogenically cooled, thus allowing it to observe multiple infrared wavelengths without much instrumental background. Having eliminated the effect of the earth’s atmosphere and the instrumental background, only the zodiacal dust in the solar system and the stellar and interstellar emissions of the Galaxy remained.

Even with the contamination of the atmosphere removed, the DIRBE data did not readily reveal an isotropic background. Removing the remaining foregrounds turned out to be a difficult task with the zodiacal dust proving to be especially difficult as none of the models were able to completely eliminate it from the data, especially in the near and mid-infrared where the dust emits and scatters the most. The emissions from interstellar dust were more readily modeled

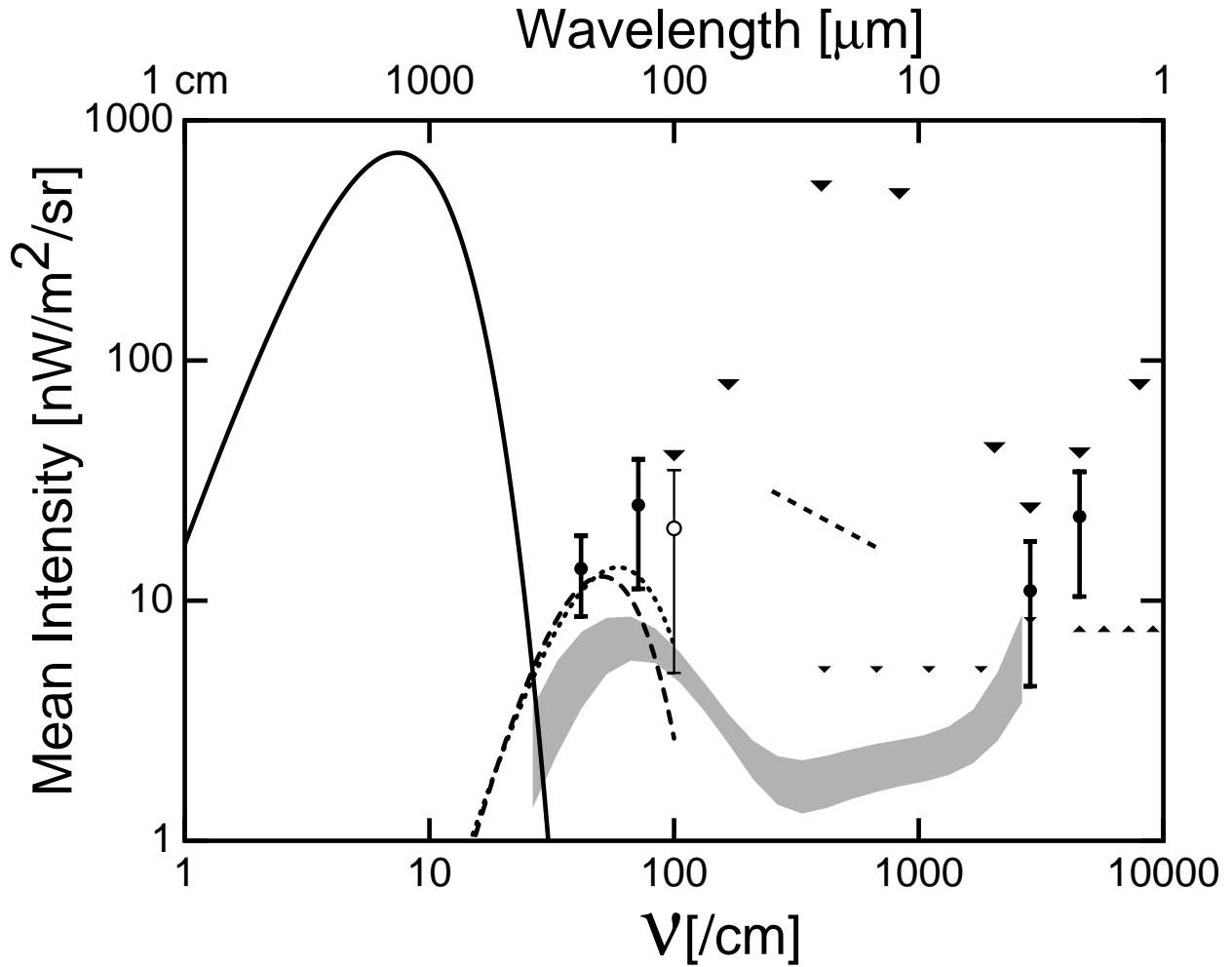


Fig. 1.— Limits and detections by DIRBE compared to various CIRB models. The DIRBE  $2\sigma$  upper limits at 1.25-60  $\mu\text{m}$ , and detections at 140  $\mu\text{m}$  and 240  $\mu\text{m}$  with  $\pm 2\sigma$  error bars are represented by solid circles. The 100  $\mu\text{m}$  intensity is represented by both the 95% confidence limit on the non-galactic, non-zodiacal intensity of 5-35  $\text{nW m}^{-2} \text{sr}^{-1}$  and the quoted upper limit on the cosmic background. The Far InfraRed Absolute Spectrophotometer (FIRAS) 125-5000  $\mu\text{m}$  detection (Fixsen *et al.* 1998) is shown by a dotted curve while the Lagache *et al.* (1999) is shown by a dashed curve; the  $\lambda < 2.2 \mu\text{m}$  lower limits of Pozzetti *et al.* (1998) are represented by small upward triangles. The upper limits on the CIRB based on TeV observations of Mrk 501 (Staney & Franceschini 1998) are shown as small downward triangles, while the “detection” based on TeV observations of Mrk 421 (Dwek & Slavin 1994) is shown as a dashed line. The gray band shows the models of Malkan & Stecker (1998).

and removed and the emissions from stars were also modeled and removed. These attempts at foreground removal finally yielded values for a CIRB at  $140\text{ }\mu\text{m}$  and  $240\text{ }\mu\text{m}$ , first as a possible detection from an independent group (Schlegel *et al.* 1998) and then the definitive value from the DIRBE science team (Hauser *et al.* 1998). These values are shown in Figure 1 in relation to various models. As can be seen, the models are within factors of 2-6 of the observed values at  $140\text{ }\mu\text{m}$  and  $240\text{ }\mu\text{m}$ , indicating a convergence between observation and theory in the far-IR.

Yet in the near-IR (NIR) ( $1 - 5\text{ }\mu\text{m}$ ), DIRBE was unable to detect the CIRB. The contamination from the zodiacal dust as well as uncertainties in the contribution of galactic stars resulted in residuals which had large error bars and thus could only be considered as upper limits (Hauser *et al.* 1998). In addition, the residual maps in the NIR failed the tests for isotropy even in limited regions of the sky.

### 1.1. Zodiacal Light Removal

The zodiacal dust is made up of dust from asteroids and comets and extends out to the asteroid belt. The particles scatter and emit light from the UV through the infrared with a minimum of the sum of scattering and emission at  $3.5\text{ }\mu\text{m}$ . In recent decades a great deal has been added to our knowledge of the zodiacal dust, especially with the advent of satellites like IRAS and COBE. Taking the sum of our knowledge today, we know that the zodiacal dust is distributed in a fan shape centered on the sun and that it is slightly tilted with respect to the ecliptic. There are dust bands associated with asteroidal families, and there is a zodiacal dust ring at a distance of 1.01 AU. Unfortunately this accumulated knowledge has not brought with it a completely accurate model of the dust distribution. The DIRBE science team has produced a model of the dust distribution (Kelsall *et al.* 1998) to subtract from the DIRBE all-sky maps, but the model parameters are not unique and thus, after subtraction, the model zodiacal light leaves some residual effects.

Kelsall *et al.* (1998) leaves a large residual intensity in the galactic polar caps at  $25\text{ }\mu\text{m}$ , the DIRBE band that is most dominated by the zodiacal light. For example, the  $25\text{ }\mu\text{m}$  intensity toward the DIRBE dark spot at  $(l, b) = (120.8^\circ, 65.9^\circ)$  in the DIRBE Zodi-Subtracted Mission Average (ZSMA) maps is  $1.76\text{ MJy sr}^{-1}$ . This cannot be a cosmic background because the lack of  $\gamma$ -ray emission toward Mkn 501 limits the CIRB to be  $< 33\text{ kJy sr}^{-1}$  (Funk *et al.* 1998). It also cannot be galactic cirrus because the  $100\text{ }\mu\text{m}$  intensity in this field is  $1.27\text{ MJy sr}^{-1}$  in the ZSMA maps, and Arendt *et al.* (1998) specify the ISM intensity as  $R(\lambda)(I(100) - I_o)$ , with  $R(25) = 0.0480$  and  $I_o = 0.66\text{ MJy sr}^{-1}$ , so the ISM intensity is  $29\text{ kJy sr}^{-1}$ . By elimination, most of this intensity must be zodiacal.

In order to reduce the residual zodiacal emission in the maps, Wright (1997) added one “observation” that the high  $b$  intensity at  $25\text{ }\mu\text{m}$  should be zero to the more than  $10^5$  observations used in the zodiacal model fitting. Even this very low weight pseudo-observation lowered the  $25\text{ }\mu\text{m}$  intensity in the dark spot to  $0.26\text{ MJy sr}^{-1}$ . This indicates that the isotropic component of the

zodiacal emission is very poorly constrained in fits that just look at the time variation to measure the zodiacal light. The Appendix in Wright (1998) discusses zodiacal light models in more depth, and the Appendix of this paper gives the actual parameters of the model we have used.

Since the residual 25  $\mu\text{m}$  intensity is now only 1% of the total zodiacal emission, we might hope for errors in the ZL model equal to 1% of the ecliptic pole intensity. But the situation is more uncertain at 2.2 and 3.5  $\mu\text{m}$  due to the scattered component of the ZL. Adjusting the thermal emission component to fit the 25  $\mu\text{m}$  intensity will not necessarily lead to a correct scattered component. So we have adopted ZL modeling errors of 5% of the intensity at the ecliptic poles at 2.2 and 3.5  $\mu\text{m}$ . These errors are slightly lower at 2.2  $\mu\text{m}$  (5.2 *vs.* 6  $\text{nW m}^{-2} \text{sr}^{-1}$ ) and higher at 3.5  $\mu\text{m}$  (2.8 *vs.* 2  $\text{nW m}^{-2} \text{sr}^{-1}$ ) than the errors adopted by Kelsall *et al.* (1998).

## 1.2. Interstellar Medium Contribution

Another foreground is the emission from dust in the interstellar medium (ISM). This contribution is significant in the FIR but is relatively small in the NIR. However, it can not be completely neglected. The distribution of the dust was modeled by Arendt *et al.* (1998) by correlating the DIRBE 100  $\mu\text{m}$  map with external data sets of gas and dust like HI, HII, and CO. Arendt *et al.* (1998) specify that the ISM subtracted map at wavelength  $\lambda$  is  $I_\nu(\lambda, l, b) - R(\lambda)(I_\nu(100, l, b) - I_\circ)$ .  $I_\circ = 0.66 \text{ MJy sr}^{-1}$  is the non-zodiacal, non-galactic component of the 100  $\mu\text{m}$  map. The coefficient  $R(2.2 \mu\text{m})$  is zero, but  $R(3.5 \mu\text{m}) = 0.00183$  (Arendt *et al.* 1998) due to single photon induced thermal fluorescence in the 3.3  $\mu\text{m}$  PAH feature in very small grains. We have made this correction on a pixel by pixel basis, and it should remove the effect of galactic cirrus if the global coefficient applies to our spot. The ISM correction listed in Table 2 is the correction averaged over the 17 pixels in the “dark spot”.

## 1.3. Foreground Starlight Removal

Since there is no all-sky map at a sufficiently high resolution in the NIR, it is difficult to calculate the cumulative intensity of stars at varying galactic locations. This calculation is vital in eliminating one of the main foregrounds to the CIRB between 1  $\mu\text{m}$  and 5  $\mu\text{m}$ .

To get an estimate of the intensity from stars, theoretical models of the Galaxy have been constructed from which number counts in any direction can be derived. The most recent and successful model of the Galaxy was an enhancement of the Wainscoat *et al.* (1992) model made by Cohen (1994) who divided the Galaxy into 5 main components: the disk, the spiral arms, the molecular ring, the central bulge, and the extended halo, as well as several minor components: Gould’s belt, local molecular clouds, reflection nebulae, etc. In his model, each major component has 82 different stellar types distributed among the components with weighting techniques designed to reproduce observations of each component in the NIR. Additionally the spectral classes are

characterized by absolute magnitudes at IR wavelengths, a magnitude dispersion, a scale height above the galactic plane, and a solar neighborhood density. Finally, dust in the Galaxy is modeled using the Rieke & Lebofsky (1985) uniform extinction law.

For the purpose of detecting the CIRB, the model has to be accurate at high galactic latitudes where the number counts are lowest and present the least amount of contamination. This is where the difficulties with the model become evident. Since the sun is situated about 15 pc above the disk and we are looking through the disk *and* the halo when we are looking at high galactic latitudes, any error in the halo-to-disk weighting will generate some error in the star counts. An additional source of error will be the actual distance of the sun above the disk. The greater the height above the disk, the lower the contribution of disk stars when looking North vs. South. These problems affect the counts and the surface brightness calculations at about the 10% level (Cohen 1996).

A different source of error arises when the inherently statistical predictions of the model are subtracted from observed data. Any model will not exactly recreate the number counts in the galactic region of interest. There will be a variance from the actual number of stars. This variance is of little consequence for dim stars since each star contributes relatively little to the overall intensity, but the variance becomes very important for the brighter stars where the flux of each individual star contributes significantly to the overall intensity.

While the zodiacal light model is intrinsically on the same flux scale as the DIRBE data, the relative calibration of the external stellar data for bright stars and models for faint stars *vs.* the DIRBE needs to be known with good accuracy. The faint star model of Arendt *et al.* (1998) used fluxes at zero magnitude of  $F_o(K) = 612.3$  Jy and  $F_o(L) = 285$  Jy (COBE DIRBE Explanatory Supplement 1998). We have checked these values by extracting the total flux in 16 pixel areas around the bright stars  $\beta$  And,  $\alpha$  Tau,  $\alpha$  Aur,  $\alpha$  Ori,  $\alpha$  Boo,  $\alpha$  Her &  $\beta$  Peg. The median  $F_o(K)$  derived from these stars is  $F_o(K) = 614$  Jy with a mean and standard deviation of the mean  $616.6 \pm 12.5$  Jy. This calibration agrees with Arendt *et al.* (1998) to better than 1%. But at  $3.5 \mu\text{m}$ , the median  $F_o(L) = 263$  Jy and the mean is  $264.9 \pm 3.4$  Jy. This is an 8% discrepancy. We will use our median value,  $F_o(L) = 263$  Jy, and specify the changes created if the Arendt *et al.* (1998) value is used instead.

Until recently, only this modeling approach was used to eliminate the galactic foreground. However, Dwek & Arendt (1998; DA98) attempted to address the uncertainty in the number counts of stars using an innovative technique. They used the zodiacal light subtracted DIRBE all-sky maps at  $2.2 \mu\text{m}$  to help determine the background at  $3.5 \mu\text{m}$ . First they subtracted a background from the  $2.2 \mu\text{m}$  data based on deep K band ( $2.2 \mu\text{m}$ ) galaxy counts. This then should have left only the stellar contribution in the  $2.2 \mu\text{m}$  maps. Then the  $1.25$ ,  $3.5$ , and  $4.9 \mu\text{m}$  maps were used to determine the proper colors of the stars which were then subtracted from the  $3.5 \mu\text{m}$  map. Based on this approach they made a tentative claim of detection for the CIRB at  $3.5 \mu\text{m}$  of:

$$\nu I_\nu(3.5 \mu\text{m}) = 9.9 + 0.312(\nu I_\nu(2.2 \mu\text{m}) - 7.4) \pm 2.9 \quad (1)$$

where  $\nu I_\nu$  is in units of  $\text{nW m}^{-2} \text{sr}^{-1}$ . The factor of 0.312 is the color correction which was found

from the correlation of the  $2.2\text{ }\mu\text{m}$  map with the  $3.5\text{ }\mu\text{m}$  map, and the  $(\nu I_\nu(2.2\text{ }\mu\text{m}) - 7.4)$  is the real value of the CIRB at K minus the assumed value of the CIRB of  $7.4\text{ nW m}^{-2}\text{ sr}^{-1}$  from the deep galaxy counts.

#### 1.4. Motivation for this Project

As mentioned earlier, the strongest constraints available on the CIRB in the NIR are the upper limits by the DIRBE science team (Hauser *et al.* 1998), and the tentative detection at  $3.5\text{ }\mu\text{m}$  by DA98 also based on DIRBE data. The DIRBE team did not make a detection claim because they did not have a significant residual signal above the uncertainties associated with the stellar subtraction and also because they had not achieved isotropy in their residual maps (Arendt *et al.* 1998). Their stellar subtraction was achieved in 2 steps. In the first step they removed all stars brighter than 15 Jy since they were bright enough to be identifiable in the low resolution DIRBE image. This translated into a brightness cutoff at K of  $4^{th}$  magnitude and at L of  $3^{rd}$  magnitude. In the second step they modeled the contribution of stars dimmer than the cutoff value using Cohen's model of the Galaxy. Our intention was to reduce those modeling uncertainties by imaging one section of sky at high resolution to a limit at least 2 orders of magnitude fainter than the Arendt *et al.* (1998) bright star cutoff. This translated into  $9^{th}$  magnitude at K and  $8^{th}$  magnitude at L. At these limits, the standard deviation in the intensity contributed by the Poisson fluctuations in the numbers of faint stars is reduced to a level 16 times smaller than the standard deviation for the Arendt *et al.* (1998) threshold.

DA98 claimed a tentative detection at  $3.5\text{ }\mu\text{m}$ . Although they seemed to have isotropy, they did have a low-level large scale gradient, probably due to zodiacal light, that remained in their images. In addition, their value at  $3.5\text{ }\mu\text{m}$  was still based on an assumed value of the CIRB at  $2.2\text{ }\mu\text{m}$  obtained from  $K$ -band galaxy counts.

Our intention here was to use a much more stringent zodiacal light subtraction routine as well as to avoid any assumption about the CIRB at other wavelengths. With these two new approaches in mind we hoped to place a much tighter constraint on the CIRB at  $2.2$  and  $3.5\text{ }\mu\text{m}$ .

## 2. Observations

### 2.1. The DIRBE Data

The primary dataset for this project was the all-sky map produced by the DIRBE instrument on the COBE satellite. DIRBE was helium cooled and observed the sky at 10 different IR wavebands from  $1.25\text{ }\mu\text{m}$  to  $240\text{ }\mu\text{m}$ . The sky was mapped onto 393,216 pixels with a pixel scale of  $0.32^\circ\text{ pixel}^{-1}$  and each pixel was observed several hundred times. The instrument was also equipped with a chopper which chopped between the sky and an internal calibrator 32 times per second. Finally, the

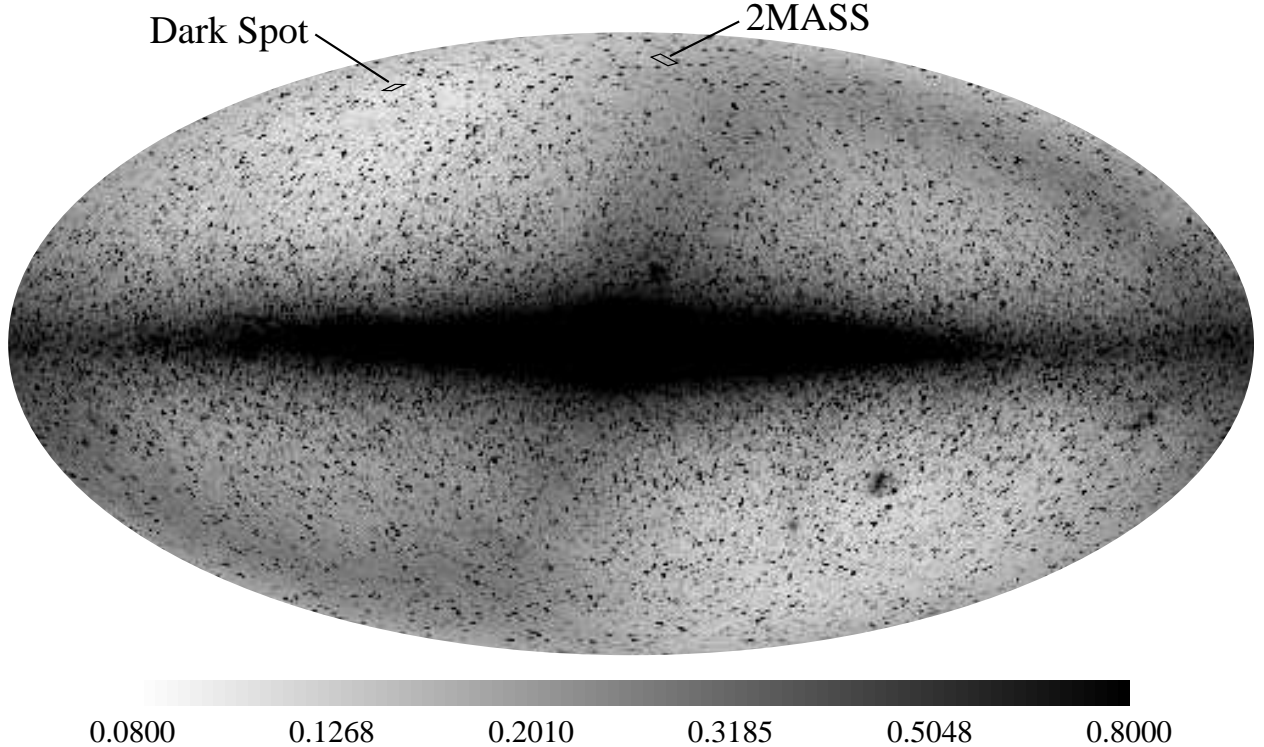


Fig. 2.— All-sky map from DIRBE at  $3.5 \mu\text{m}$  in galactic coordinates with intensities in  $\text{MJy sr}^{-1}$ . The S-shape of the zodiacal light is evident as well as the contamination of stars which appear almost as noise on the images. The “dark spot” ( $\alpha = 12^h 56.9^m$ ,  $\delta = 51^\circ 11'$  (J2000)) and the region used for the 2MASS analysis ( $\alpha = 13^h 24^m$ ,  $\delta = 15^\circ$  (J2000)) are outlined.

instrument was re-calibrated 5 times per orbit. All this redundancy resulted in the best absolutely calibrated map of the infrared sky obtained to date (Figure 2).

The first step in determining the CIRB from the DIRBE data was to determine the location in the sky with the lowest intensity. But since the Earth sits within the zodiacal dust cloud, the region of lowest emission was still heavily contaminated by scattering and emission from that dust. Figure 2 shows the prominent S-shape (in galactic coordinates) of the zodiacal dust, and before anything else could be attempted with the data, that contamination needed to be removed. To remove the contribution of the zodiacal light required modeling the distribution of the dust as well as its emission and scattering characteristics. This task was accomplished by Wright (1998) resulting in maps where the remaining contamination was from the Galaxy. We did not use the zodi-subtracted maps generated by the DIRBE science team (Kelsall *et al.* 1998) because this model leaves a large residual  $25 \mu\text{m}$  intensity in the region of our ground-based survey. Thus we used a model constructed using the “very strong no-zodi” condition defined by Wright (1997), which reduces the residual  $25 \mu\text{m}$  intensity by a factor of 7.

From the cleaned map, the area of lowest emission, a “dark spot”, was chosen which was a

region spanning 2 degrees by 2 degrees. This  $2^\circ \times 2^\circ$  area of lowest emission turned out to be near the North Galactic Pole at  $\alpha = 12^h 56.9^m$ , and  $\delta = 51^\circ 11'$  (J2000) ( $l = 120.8^\circ$ ,  $b = 65.9^\circ$ ). The low value at this location represents a combination of the CIRB and the unresolved stars within the large ( $0.7^\circ$ ) DIRBE beam. The next step was then to determine the contribution from unresolved stars using higher resolution ground based imaging.

## 2.2. The Initial Map

Obtaining the fluxes of stars in the determined “dark spot” at  $3.5 \mu\text{m}$  was the primary goal of this project, but mosaicing an area of 4 square degrees is not possible with present day technology. Modern arrays do not read out fast enough to be able to image a large region of sky before the background at  $3.5 \mu\text{m}$  saturates the array; therefore, most cameras that are meant to image in the thermal infrared ( $> 3 \mu\text{m}$ ) are designed to either image a very small region of sky to minimize the background or to read-out only a small subarray of the detector chip.

The main camera available for this project was the UCLA Twin Channel Infrared Camera (known locally as Gemini) (McLean *et al.* 1993) which mounts onto the Lick 3-m telescope. On the 3-m, Gemini’s two  $256 \times 256$  arrays have identical 3 arcminute fields of view, one array covering the wavelength range from 1 to  $2.5 \mu\text{m}$  with a HgCdTe array, and the other array covering the wavelength range from 1 to  $5 \mu\text{m}$  with an InSb array. The camera employs the subarray technique for readout when imaging at wavelengths longer than  $3 \mu\text{m}$  outputting  $64 \times 64$  pixels giving it a field of view of only  $45'' \times 45''$ . With a field of view this small it would be impossible to mosaic the required area of the “dark spot” which covers the equivalent area of 20 full moons.

The solution that was employed was to image the area at K with a different camera which due to the lower sky background at K, could have a much larger field of view, then choose the brightest stars from that sample to re-image at  $3.5 \mu\text{m}$  with Gemini on the 3-m. The camera available for this approach was the Lick InfraRed Camera 2 (LIRC2). LIRC2 could mount onto the 1-m telescope at Lick and have a field of view of  $7.29' \times 7.29'$ , easily allowing the 4 square degrees to be mapped in a short period of time. This was done over the nights of 1997, March 28 and 29. The 302 stars catalogued in the LIRC2 survey are shown in Figure 3.

The process was complicated during the reduction of the LIRC2 data when it was discovered that LIRC2 had photometric problems which precluded highly accurate photometry. The accuracy was still sufficient to estimate relative brightnesses, which was the main result that was required of the data. Having obtained the list of stars from the brightest to the dimmest in the “dark spot” we could now proceed with imaging them in the L band.

### 2.3. The Main NIR data

We had three clear and photometric nights at the Lick 3-m with Gemini on the nights of 1999, March 26 to 28. Using Gemini's twin arrays we imaged our list of stars in both the K band and the L band simultaneously.

The data were reduced using standard data reduction routines with the IRAF<sup>1</sup> software package. Since the sky brightness varies dramatically over very short periods of time at  $3.5\text{ }\mu\text{m}$ , differencing of sequential images was used in the data reduction to remove detector signature and sky background. Each star was imaged at 4 different locations on the array, while the 10 brightest stars were imaged a total of 12 times.

We also obtained time at the 1.5-m telescope at Palomar on the night of 1999, April 4, using its IR camera. We imaged the 20 brightest stars at K band as a check of our Gemini data as well as imaging the list at J band. These data were reduced in a similar fashion to the Gemini data. The uncertainties for both data sets were determined by the standard deviation of the brightness of the standard star throughout the night.

A total of 77 stars out of the original sample of 302 were observed either at Palomar or with Gemini or both. We have restricted our analysis to the brightest part of the sample in order to have a reliable catalog with a well defined limit. Table 1 shows the 28 bright stars with  $m < 9$  in the dark spot, with the original LIRC2 K magnitude, the Palomar J and K magnitudes (J60 and K60) and the Lick Gemini K and L magnitudes. We have used the Lick K and L magnitudes in this paper.

## 3. Combining the two Datasets

Having obtained the photometry from the ground for the bright stars, the task was to match up the ground based data to the space based data. Figure 3 shows a projection of the DIRBE pixels on the “dark spot” as well as the stars imaged by LIRC2.

The most obvious difficulty turns out to be that the DIRBE pixels are not aligned with the EW and NS axes; therefore, some only partially enter the  $2^\circ \times 2^\circ$  box. Also the values within the pixels themselves represent the average intensity seen when the  $0.7^\circ$  square DIRBE beam is centered within the pixel boundary, and hence are affected by the pixels around them since the beam does not abruptly stop at the edge of the pixel.

To compute the response in a given pixel to a given star, we found the probability that the star

---

<sup>1</sup>IRAF ( Image Reduction and Analysis Facility) is distributed by the National Optical Astronomy Observatories, which are operated by the Association for Research in Astronomy, Inc., under cooperative agreement with the National Science Foundation.

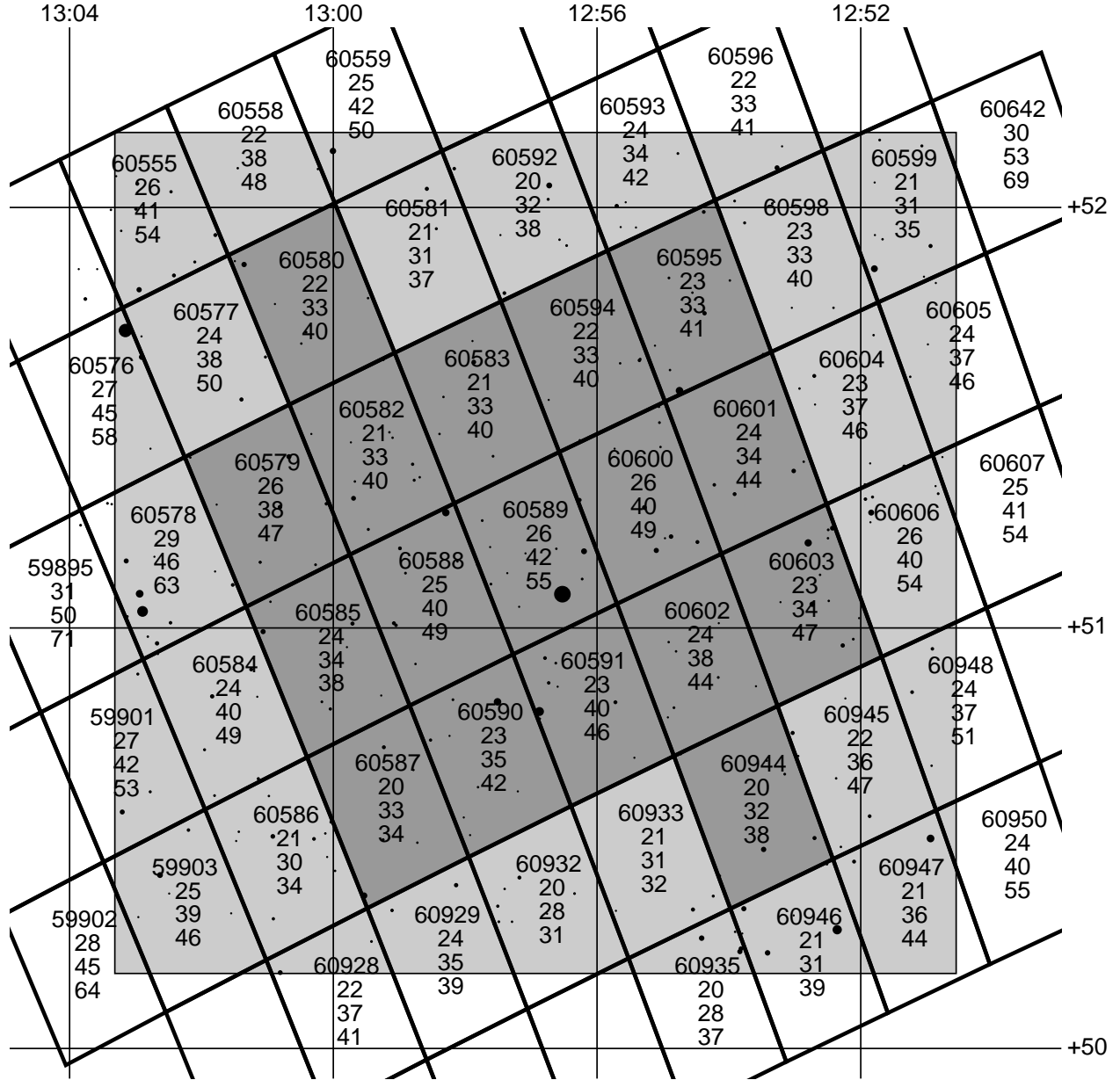


Fig. 3.— A superposition of the stars within the surveyed  $2^\circ \times 2^\circ$  area (thin-lined box gray box) and the DIRBE pixels (thick-lined skewed rectangles). The 17 DIRBE pixels used in our analysis are shaded in darker gray. The numbers in the pixels are from the top: The DIRBE pixel number and the J, K, and L intensities in  $\text{kJy sr}^{-1}$ . The grid lines are at even degrees of  $\alpha$  and  $\delta$ . The circles are the stars imaged with LIRC2. The bigger the size, the higher the flux.

was inside the DIRBE  $0.7^\circ$  square beam assuming that the beam center was uniformly distributed inside the pixel, and that the beam orientation was uniform in angle. This is a fair assumption since each pixel was observed hundreds of times in many different angles during the lifetime of the mission. To be specific, let  $H(\hat{b}, \theta, \hat{s})$  be 1 if the star with position given by the unit vector  $\hat{s}$  is in the square beam when it is centered at position  $\hat{b}$  and oriented with position angle  $\theta$ , and 0 if the star is not in the beam. Then the probability of the  $j^{th}$  star being in data taken in the  $i^{th}$  pixel is given by

$$p_{ij} = \frac{\int_0^{2\pi} \int_{\hat{b} \in \Omega_i} H(\hat{b}, \theta, \hat{s}_j) d^2\hat{b} d\theta}{2\pi \int_{\hat{b} \in \Omega_i} d^2\hat{b}} \quad (2)$$

where  $\Omega_i$  is the angular extent of the  $i^{th}$  pixel. Then the predicted contribution from bright stars to the intensity in the  $i^{th}$  pixel is given by

$$B_i = \Omega^{-1} \sum_j p_{ij} F_j \quad (3)$$

where  $\Omega$  is the solid angle of the DIRBE beam and  $F_j$  is the flux of the  $j^{th}$  star. We also need to know the variance of the intensity in the pixel due to the random orientations and random placements of observations with the pixel boundaries. This can be obtained from the expected value of  $H^2$  within a pixel, but since  $H^2 = H$  we find that the variance of  $p_{ij}$  is given by  $p_{ij}(1 - p_{ij})$ . Thus stars at the edge of the beam ( $p \simeq 0.5$ ) make the greatest contribution to the variance, a phenomenon known as “flicker noise”. We then get

$$\sigma(B_i)^2 = \Omega^{-2} \sum_j [p_{ij}(1 - p_{ij}) + p_{ij}^2 \epsilon^2] F_j^2 \quad (4)$$

where  $\epsilon$  is an uncertainty in cross-calibrating the DIRBE and ground-based data for individual stars which also includes an allowance for variability in the stars. We use  $\epsilon^2 = 0.1$  in this work. Many IR bright stars are long period variables and will not have the same flux during the DIRBE observations as they have nine years later during our ground-based survey, so a fairly large value of  $\epsilon^2$  is appropriate. Note that the variance sum is dominated by the brightest stars, and is minimized in the “dark spot”.

We have evaluated the bright star contribution for all stars with  $K < 9$  mag or  $L < 9$  mag in the dark spot. Note that the cutoff magnitude does not come from LIRC2 so as to avoid any additional error being introduced because of LIRC2’s photometric inaccuracy in the final result. Stars were detected below these limits with accurate photometry but were not used, with the conservative cut-off being at 9th magnitude. There are only 17 DIRBE pixels whose response to a uniform illumination pattern is at least 90% due to radiation from within the dark spot, and these 17 pixels form our DIRBE sample. Given the DIRBE data  $D_i$  and the bright star intensity  $B_i$ , we can estimate the cosmic infrared background using  $C_i = D_i - B_i - F - Z$ , where  $F$  is the contribution from faint stars evaluated from star count models, and  $Z$  is the zodiacal contribution. Both  $F$  and  $Z$  are essentially constant over our spot and thus are not subscripted by pixel. We

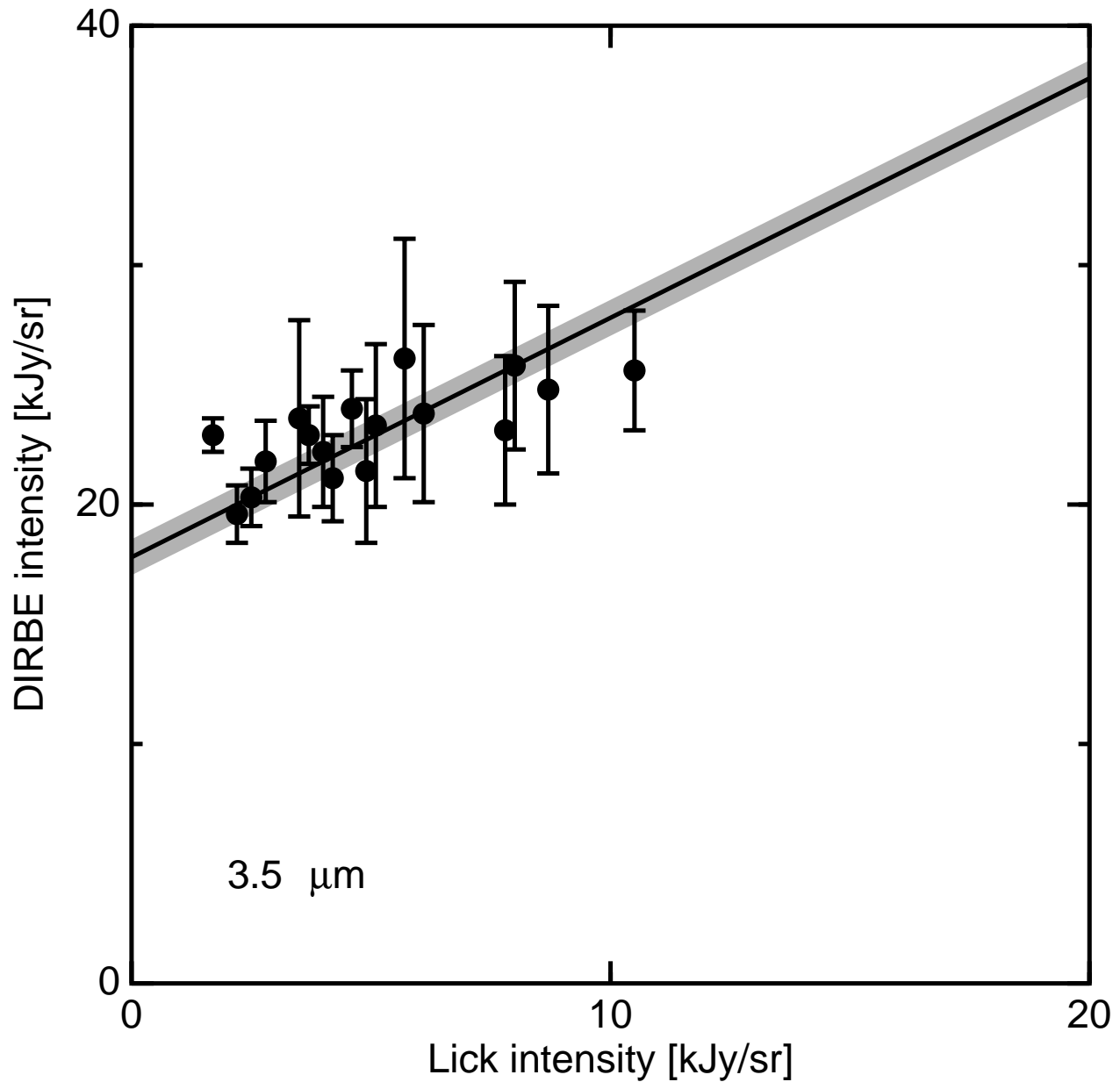


Fig. 4.— The zodi-subtracted DIRBE 3.5  $\mu$ m intensity plotted *vs.* the predicted intensity from bright stars based on Lick data for stars with  $L < 9$  mag in the dark spot at  $(l, b) = (120.8^\circ, 65.9^\circ)$ . The line is of unit slope.

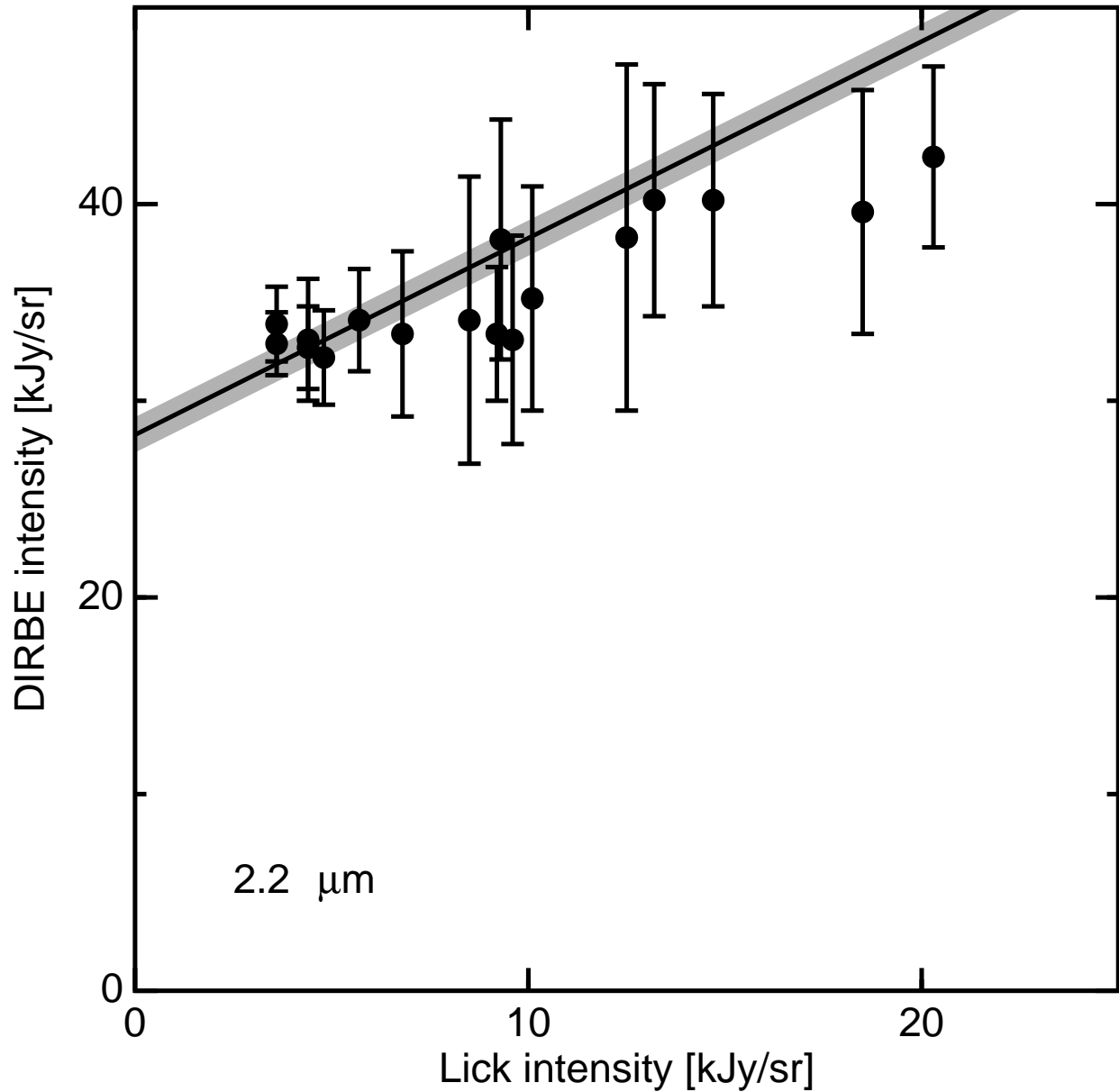


Fig. 5.— The zodi-subtracted DIRBE  $2.2 \mu\text{m}$  intensity plotted *vs.* the predicted intensity from bright stars based on Lick data for stars with  $K < 9$  mag in the dark spot at  $(l, b) = (120.8^\circ, 65.9^\circ)$ . The line is of unit slope.

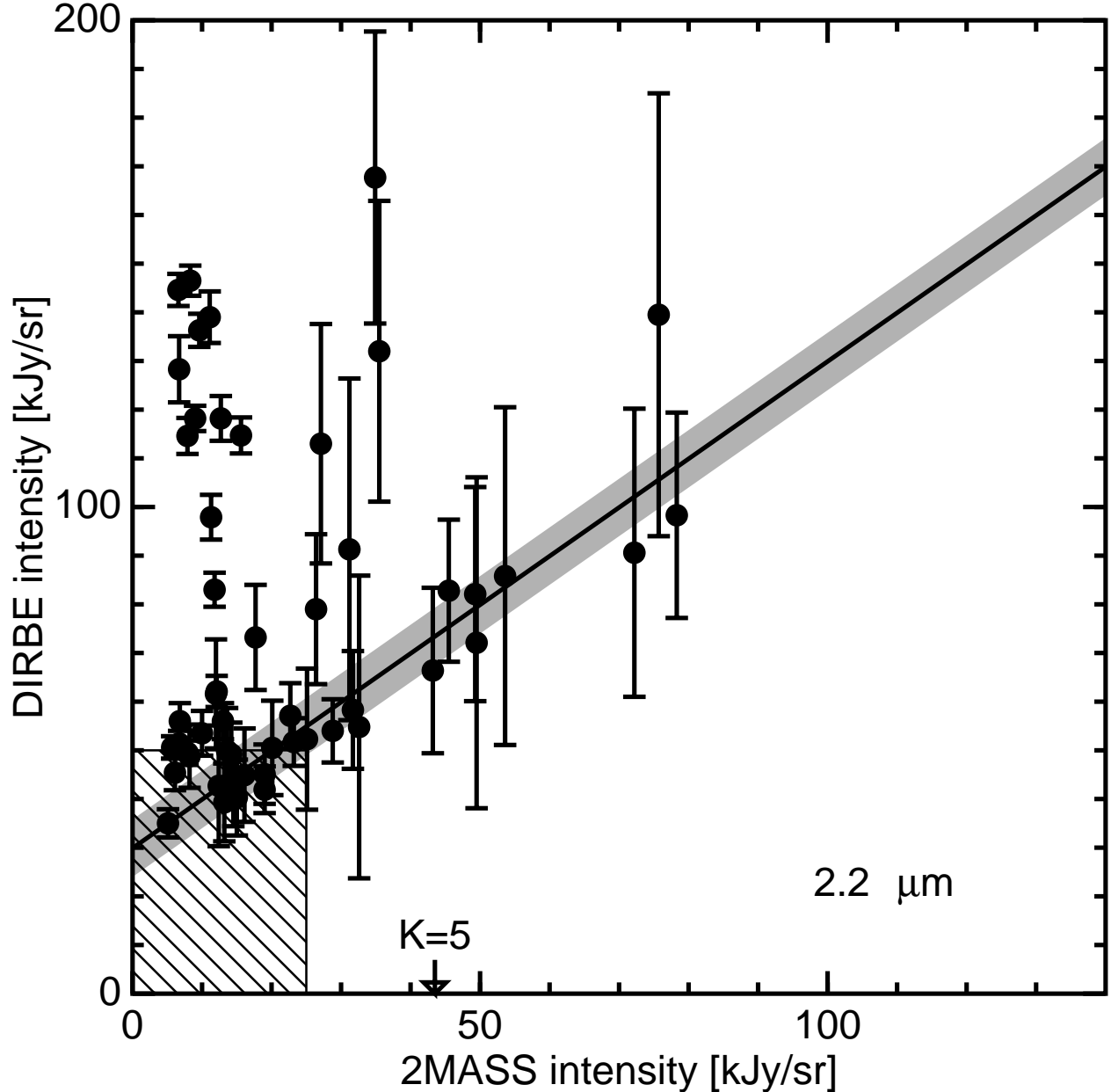


Fig. 6.— The zodi-subtracted DIRBE 2.2  $\mu$ m intensity plotted *vs.* the predicted intensity from bright stars based on 2MASS stars with  $K < 9$  mag in the region at  $(l, b) = (337.1^\circ, 75.6^\circ)$ . The arrow labeled K=5 shows the intensity produced by a single 5<sup>th</sup> magnitude star in the DIRBE beam. The cross-hatched area in the lower left shows the plotting box for Figure 5. The line is of unit slope and the intercept is in good agreement with our value for the intensity from stars  $K > 9$  mag plus the CIRB.

combine the several estimates of the cosmic infrared background using a weighted median: we find the value  $\hat{C}$  that minimizes

$$E = \sum_i \left| \frac{C_i - \hat{C}}{\sigma(B_i)} \right| \quad (5)$$

The uncertainty in  $\hat{C}$  is found using the half-sample method (Babu & Feigelson 1996): many Monte Carlo runs were performed each with a randomly chosen half of the pixels, and the scatter in these determinations gives the uncertainty in  $\hat{C}$ . The result for the CIRB plus the faint stars ( $\hat{C} + F$ ) at K is  $28.27 \pm 0.90$  kJy sr $^{-1}$ , and at L is  $17.81 \pm 0.75$  kJy sr $^{-1}$ . These uncertainties are based only on the statistical pixel to pixel scatter within the “dark spot”, but they do include the fluctuations in the faint star contribution. Figure 4 shows the zodi-subtracted DIRBE 3.5  $\mu$ m intensity,  $D_i - Z$ , plotted against the bright star intensity predicted from the Lick L band data. The slope of a line fitted to these points is only 0.4, but this does not mean that the DIRBE calibration differs by a factor of 0.4 from the ground-based calibration. Rather it shows that the variance of the stellar contribution is not dominated by the bright stars in this “dark spot”, and thus the predicted stellar intensity is a noisy estimator of the actual stellar intensity. In this circumstance, the slope of a least-squares line is biased low, as shown in Figure 2 of Wright (1992). Figure 6 shows a similar plot using 2MASS data in a  $2.4^\circ \times 4^\circ$  region centered at  $\alpha = 13^h 24^m$ ,  $\delta = 15^\circ$ . This region is at high galactic latitude ( $l = 337^\circ$ ,  $b = 76^\circ$ ) but has not been selected to have very few bright stars. Even though pixels affected by stars listed as saturated in the 2MASS catalog have been deleted, there appear to be several stars that are partially saturated in the 2MASS data leading to pixels with high DIRBE intensities but low 2MASS intensities. However, the plotted line with unit slope is clearly consistent with a large number of pixels. The intercept is  $29.9 \pm 5.9$  kJy sr $^{-1}$  which compares very well with the  $28.3 \pm 0.9$  kJy sr $^{-1}$  found in the “dark spot”.

The 17 pixels are not independent because a given star affects several pixels. The ratio of the  $0.7^\circ$  square beam solid angle to the pixel solid angle is 4.7:1. But the effective beam has fuzzy edges where  $p_{ij}$  is close to 0.5, and the appropriate beam solid angle to use is the noise effective solid angle  $\Omega_e = (\sum_i p_{ij})^2 / \sum_i p_{ij}^2 = 6$  pixels (Wright 1985). We therefore multiply the statistical uncertainty given above by a factor of  $\sqrt{6} \approx 2.5$ , giving the error bars on the  $m < 9$  contribution listed in Table 2. But this uncertainty also includes the  $\sqrt{N}$  fluctuations in the faint stars and any DIRBE instrument noise.

We have run the Wainscoat *et al.* (1992) star count model for the “dark spot” and our 2MASS region. In the 2MASS region the model predicts 785 stars with  $9 < K < 12$  mag and we find 704 stars. Thus the model count is  $11.5\% \pm 3.8\%$  too high. The predicted integrated intensity from stars with  $9 < K < 12$  mag is  $11.2\% \pm 5.4\%$  too high. This 11% difference is well within the 10-15% estimated uncertainty in the model (Arendt *et al.* 1998). In the absence of data similar to 2MASS at 3.5  $\mu$ m, we assume that the model colors are correct, and apply this correction factor to the model values for the contribution from stars fainter than 9<sup>th</sup> magnitude in the “dark spot” at both 2.2  $\mu$ m and 3.5  $\mu$ m and get  $F = 11.9 \pm 0.6$  kJy sr $^{-1}$  at K and  $F = 5.7 \pm 0.3$  kJy sr $^{-1}$  at L.

There is a bias in  $F$  introduced by our selection of a “dark spot”. Let the total flux which we

select on be  $T = B + F$ , where the bright star contribution  $B$  and the faint star contribution  $F$  are independent random variables. If  $B$  and  $F$  are Gaussian, and we select on  $T$ , then there is a bias in  $F$  of  $\sigma_F \times (\sigma_F/\sigma_T) \times (T/\sigma_T)$ . We have selected a dark spot that is a fluctuation with probability of  $\sim 10^{-4}$ . The actual fluctuations are not Gaussian, and  $B$  has infinite variance, but if we limit  $T$  to stars fainter than the 15 Jy cutoff used by Arendt *et al.* (1998) a Gaussian approximation is not too bad. Then  $P = 10^{-4}$  is a  $-4\sigma$  selection. At  $2.2 \mu\text{m}$ ,  $\sigma_T = 10.8 \text{ kJy sr}^{-1}$  and  $\sigma_F = 0.66 \text{ kJy sr}^{-1}$  in a  $2^\circ \times 2^\circ$  box, leading to a bias in  $F$  of  $0.66 \times (0.66/10.8) \times (-4) = -0.16 \text{ kJy sr}^{-1}$ . At  $3.5 \mu\text{m}$ ,  $\sigma_T = 8.8 \text{ kJy sr}^{-1}$  and  $\sigma_F = 0.32 \text{ kJy sr}^{-1}$ , leading to a bias in  $F$  of  $-0.05 \text{ kJy sr}^{-1}$ . We have not corrected for these biases, but in principle our CIRB results should be increased by  $0.16 \text{ kJy sr}^{-1}$  at  $2.2 \mu\text{m}$  and  $0.05 \text{ kJy sr}^{-1}$  at  $3.5 \mu\text{m}$ .

There is an ISM component at  $3.5 \mu\text{m}$  that also needs to be subtracted. It is 0.00183 times the difference between the zodi-subtracted  $100 \mu\text{m}$  intensity, which has a mean of  $I_{100} = 1.02 \text{ MJy sr}^{-1}$  in our “dark spot”, and the zero  $N_H$  intercept of the  $I_{100}$  *vs.*  $N_H$  correlation, which is  $I_o = 0.66 \text{ MJy sr}^{-1}$  (Arendt *et al.* 1998). Our maps used for the pixel by pixel bright star fitting had 0.00183 times the *entire* zodi-subtracted  $100 \mu\text{m}$  intensity subtracted without first removing  $I_o$ . Furthermore,  $I_o$  using our zodi model would be  $0.4 \text{ MJy sr}^{-1}$  since we subtracted more zodi. Since we used  $I_{3.5} - 0.00183I_{100}$  but want  $I_{3.5} - 0.00183(I_{100} - I_o)$ , we need to add a constant  $0.00183I_o = 0.7 \text{ kJy sr}^{-1}$  to our  $3.5 \mu\text{m}$  results to complete the ISM correction.

Noise due to the DIRBE detectors would be included in the pixel to pixel scatter, but independent from pixel to pixel. Thus the contribution from DIRBE noise should not be multiplied by the factor of 2.5 discussed above, and we have been conservative by assuming that the DIRBE noise is zero. There is no calibration error between DIRBE and the zodiacal light models since the models are fit to data on the DIRBE scale.

Other errors could potentially arise from the zodiacal modeling uncertainties and the cross calibration uncertainties between the ground based and space based data. These uncertainties are dominated by errors in the zodiacal cloud model, and we estimate them to be  $3.8 \text{ kJy sr}^{-1}$  at  $2.2 \mu\text{m}$  and  $3.3 \text{ kJy sr}^{-1}$  at  $3.5 \mu\text{m}$ . Taking the quadrature sum of 2.5 times the statistical error and our estimated zodiacal modeling errors gives a net uncertainty of  $4.4 \text{ kJy sr}^{-1}$  at  $2.2 \mu\text{m}$  and  $3.8 \text{ kJy sr}^{-1}$  at  $3.5 \mu\text{m}$ .

Having determined the stellar contribution we removed it from the DIRBE map arriving at a residual signal at K of:

$$I_{2.2\mu\text{m}} = 16.4 \pm 4.4 \text{ kJy sr}^{-1} \quad (6)$$

or

$$\nu I_{2.2\mu\text{m}} = 22.4 \pm 6.0 \text{ nW m}^{-2} \text{ sr}^{-1} \quad (7)$$

and a signal at L of:

$$I_{3.5\mu\text{m}} = 12.8 \pm 3.8 \text{ kJy sr}^{-1} \quad (8)$$

or

$$\nu I_{3.5\mu\text{m}} = 11.0 \pm 3.3 \text{ nW m}^{-2} \text{ sr}^{-1} \quad (9)$$

Table 2 shows the total DIRBE intensities and the zodiacal light, interstellar medium, bright stars, faint stars, and the residual signal. It should be emphasized that using the Kelsall *et al.* (1998) zodiacal light model instead of our model gives a residual intensity that is 5.1 kJy sr<sup>-1</sup> higher at 3.5  $\mu$ m and 6.6 kJy sr<sup>-1</sup> higher at 2.2  $\mu$ m.

Using the DIRBE faint source model calibration of  $F_o(L) = 285$  Jy instead of the  $F_o(L) = 263$  Jy we measured would reduce the derived residual intensity at 3.5  $\mu$ m by 0.74 kJy sr<sup>-1</sup>.

#### 4. Discussion

The technique of zodiacal light subtraction used in this paper reduces the possibility that this residual signal is an artifact of this model. Certainly replacing our zodi model by the Kelsall *et al.* (1998) model would increase the apparent statistical significance of our result, but would leave an unexplained high latitude residual in the 25  $\mu$ m map. Our mapping of the dark spot also eliminates the possibility that the signal is stellar in origin: by observing and directly subtracting stars down to 9<sup>th</sup> magnitude we reduce our dependence on the Wainscoat *et al.* (1992) starcount model by a factor of 4 relative to the analysis of Arendt *et al.* (1998) and Hauser *et al.* (1998). Hence we conclude that the residual signal is the CIRB.

Since we have only observed 0.01% of the sky, we cannot directly verify the isotropy of the CIRB that we see. But the evidence we do have for isotropy at 3.5  $\mu$ m is qualitatively the same kind of evidence that Hauser *et al.* (1998) had for isotropy of CIRB at 240  $\mu$ m. The 240  $\mu$ m map is *NOT* isotropic, but  $I_{240} - R(240)(I_{100} - I_o)$  is. Finding the level of this isotropic signal requires a determination of  $I_o$  by carefully subtracting the galactic signal in a “dark spot”: the Lockman hole. DA98 show that  $I_{3.5} - 0.312(I_{2.2} - I_o)$  is isotropic, and obtained a lower limit on  $I_o$  using galaxy counts. We have determined the value of  $I_o$  by carefully subtracting the galactic signal in our dark spot. Thus the Hauser *et al.* (1998) determination of the far-infrared CIRB and our determination of the near-infrared CIRB are logically equivalent. But one has more confidence in the Hauser *et al.* (1998) result because Arendt *et al.* (1998) were able to determine their  $I_o$  at 100  $\mu$ m in 3 areas with consistent results.

Although the uncertainty for the 2MASS spot is large, we find that the value of the residual signal derived from the “dark spot” agrees with the 2MASS spot. In the future, we will be able to further verify the isotropic nature of this signal. Since 2MASS saturates on stars that are quite faint for DIRBE, 2MASS data can only be used in regions with no bright stars. The current 2MASS data release does not cover any of our DIRBE dark spots. However, future data releases will eventually cover the whole sky, allowing a good isotropy check on the CIRB at 2.2  $\mu$ m.

Our accepted proposal to survey the darkest spot in the Southern sky at the South Pole SPIREX/ABU facility in the 3.5  $\mu$ m band during the 1999 austral winter was not executed due to equipment problems. Surveying other dark spots at 3.5  $\mu$ m would be very valuable but also very difficult with ground-based telescopes.

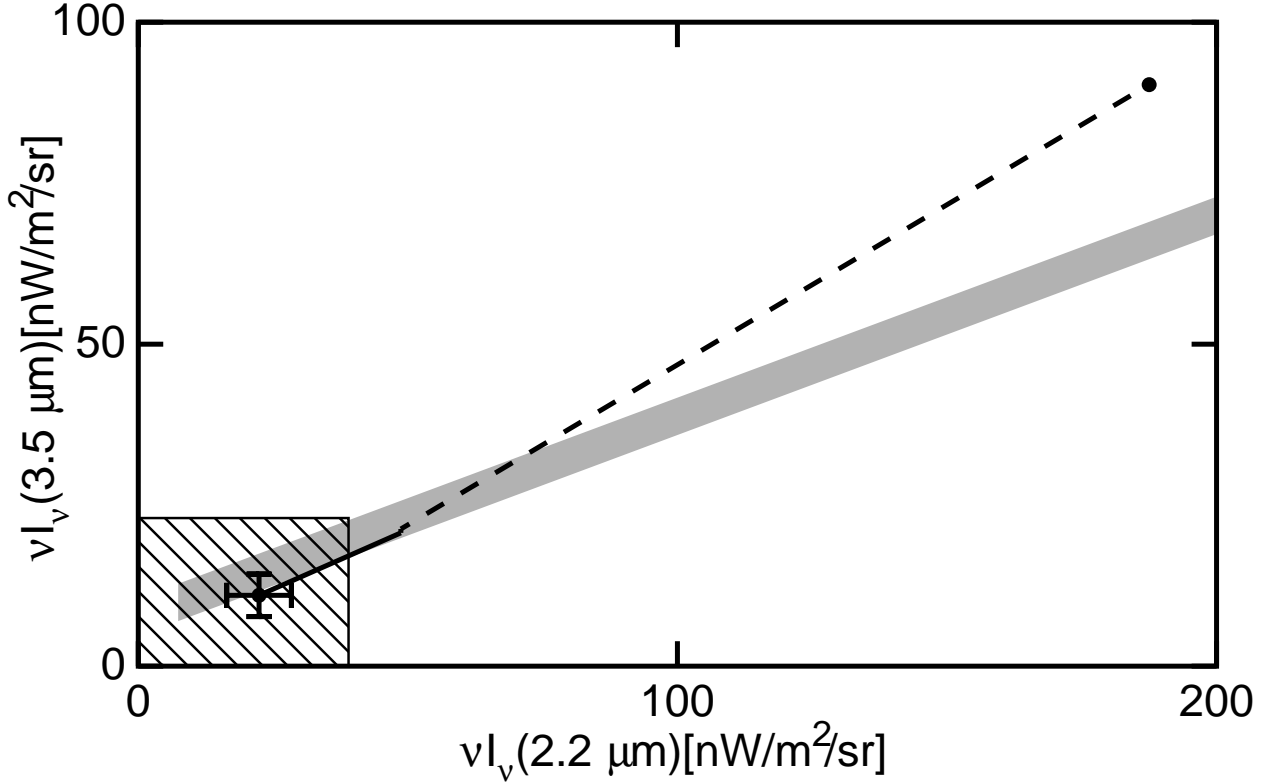


Fig. 7.— Comparison of our results (point with error bars) and previous limits: the hatched region shows the Hauser *et al.* (1998) upper limits, while the gray bar shows the DA98 correlation. The point in the upper right shows the actual average DIRBE intensity in our 17 pixel dark spot, with the dashed line showing the zodiacal light subtraction, and the solid line showing the star light subtraction.

Even though our evidence for the isotropy of the near infrared background is not strong, the uncertainty in our final result is still dominated by the uncertainties in modeling the zodiacal light. Our CIRB values at both 2.2 and 3.5  $\mu\text{m}$  are 19% of the zodiacal light at the ecliptic poles, while the 240  $\mu\text{m}$  background found by Hauser *et al.* (1998) is 3.6 times larger than the zodiacal light at the ecliptic poles. Thus the near IR background is much more sensitive to zodiacal light errors than the far IR background.

## 5. Conclusion

We compare our values to the values obtained by Hauser *et al.* (1998), and DA98 in Figure 7. Hauser *et al.* (1998) made no claim for the CIRB since they did not get isotropy over a large part of the sky. However they did publish values for regions of the sky where all foreground contaminations were expected to be lowest. They labeled them as high quality (HQ) regions. HQA

covered approximately 20% of the sky and HQB covered approximately 2% of the sky. Their HQA value at K was  $9.5 \pm 8.8$  kJy sr $^{-1}$  ( $13 \pm 12$  nW m $^{-2}$  sr $^{-1}$ ) while their HQB values was  $10.9 \pm 8.8$  kJy sr $^{-1}$  ( $14.9 \pm 12$  nW m $^{-2}$  sr $^{-1}$ ), where the uncertainties are the systematic errors. Our value falls within one sigma of both their HQA and HQB values though that is due mostly to the fact that their error bars are very large.

At L band their HQA value was  $13 \pm 7$  kJy sr $^{-1}$  ( $11 \pm 6$  nW m $^{-2}$  sr $^{-1}$ ) and their HQB value was  $13.3 \pm 7$  kJy sr $^{-1}$  ( $11.4 \pm 6$  nW m $^{-2}$  sr $^{-1}$ ). Our L band value is also within one sigma though much closer to their quoted numbers.

Since DA98 were able to make a much more precise measure than Hauser *et al.* (1998), the comparison between our value and theirs is very interesting. Inserting our value for  $\nu I_\nu(2.2 \mu\text{m})$  into the DA98 correlation predicts  $\nu I_\nu(3.5 \mu\text{m}) = (13.8 \pm 3.5)$  nW m $^{-2}$  sr $^{-1}$  which is one standard deviation higher than our result. Note that DA98 essentially only determined that the high galactic latitude intensity could not be entirely due to galactic stars because a smooth component with a redder K-L color was needed. In principle, this “horse of a different color” could have been incompletely subtracted zodiacal light, since the K-L color of the zodiacal light is much redder than typical stars due to the contribution of thermal emission to the  $3.5 \mu\text{m}$  intensity. If we had used the Kelsall *et al.* (1998) zodiacal light model instead of our own, the inferred  $2.2 \mu\text{m}$  CIRB would have increased by 6.6 kJy sr $^{-1}$  and the  $3.5 \mu\text{m}$  CIRB would have increased by 5.1 kJy sr $^{-1}$ . These changes would have induced a change of  $3 \times (5.1/3.5 - 0.312 \times 6.6/2.2) = 1.6$  nW m $^{-2}$  sr $^{-1}$  in the difference between the DA98 result and our result, in the sense that the difference would go from  $(3.5 \pm 3.5)$  nW m $^{-2}$  sr $^{-1}$  to  $(1.9 \pm 3.5)$  nW m $^{-2}$  sr $^{-1}$ . Thus our values are in very good agreement with the DA98 correlation. Since we use a different zodiacal light model and a different method of star subtraction, the fact that we and DA98 have arrived at similar numbers gives confidence that the residual signal we derive at  $2.2 \mu\text{m}$  and  $3.5 \mu\text{m}$  is very likely the CIRB rather than an unknown component of Galactic emission.

The COBE datasets were developed by the NASA Goddard Space Flight Center under the guidance of the COBE Science Working Group and were provided by the NSSDC. This publication makes use of data products from the Two Micron All Sky Survey, which is a joint project of the University of Massachusetts and the Infrared Processing and Analysis Center, funded by the National Aeronautics and Space Administration and the National Science Foundation.

## A. Zodiacal Light Model

The zodiacal light model used in this paper is derived from the model described in Wright (1998). Three changes have been made:

1. The scattering phase function coefficients  $p_{20}$  and  $p_{21}$  are allowed to be different for each of

the three short wavelength bands. In Table 3, I use JKL to distinguish the values for the 1.25, 2.2 and 3.5  $\mu\text{m}$  bands.

2. The scaling of the IRAS zodiacal bands,  $p_{13}$ , is allowed to be different for the scattered light, denoted  $p_{13S}$ , than it is for the thermal emission, denoted  $p_{13T}$ .
3. The model was fit to the “very strong no zodi” condition of Wright (1997).

The emissivities are given in Table 4 and the IRAS band parameters are given in Table 5.

## REFERENCES

Arendt, R., *et al.* 1998, ApJ, 508, 74

Babu, G. J. & Feigelson, E. 1996, “Astrostatistics”, CRC Press

Boggess, N. W. 1992, ApJ, 397, 420

Bond, J. R., Carr, B. J. & Hogan, C. J. 1986, ApJ, 306, 428

Bond, J. R., Carr, B. J. & Hogan, C. J. 1991, ApJ, 367, 420

COBE Diffuse Infrared Background Experiment (DIRBE) Explanatory Supplement, Version 2.3. 1998, ed. M. G. Hauser, T. Kelsall, D. Leisawitz, & J. Weiland (COBE Ref. Pub. 97-A; Greenbelt: NASA/GSFC), available in electronic form from the NSSDC at <http://www.gsfc.nasa.gov/astro/cobe/cobehome.html>

Cohen, M. 1994, AJ, 107, 582

Cohen, M. 1996, in AIP Conf. Proc. 348, Unveiling the Cosmic Infrared Background, ed. E. Dwek (New York: AIP), 67

Dwek, E. & Arendt, R. 1998, ApJ, 508, L9 (DA98)

Dwek, E. & Slavin, J. 1994, ApJ, 436, 696

Fabbri, R., Andreani, P., Melchiorri, F. & Nishi, B. 1987, ApJ, 315, 12

Fabbri, R. 1988, ApJ, 334, 6

Fixsen, D., Dwek, E., Mather, J. Bennett, C. & Shafer, R. 1998, ApJ, 508, 123

Funk, B., Magnussen, N., Meyer, H., Rhode, W., Westerhoff, S. & Wiebel-Sooth, B. 1998, Astroparticle Physics, 9, 97

Hauser, M. G. 1996, in AIP Conf. Proc. 348, Unveiling the Cosmic Infrared Background, ed. E. Dwek (New York: AIP), 11

Hauser, M. *et al.* 1998, ApJ, 508, 25

Harwit, M. 1970, Rivista del Nuevo Cimento, vol II, 253

Kaufman, M. 1976, Ap&SS, 40, 469

Kelsall, T. *et al.* 1998, ApJ, 508, 44

Lagache, G., Abergel, A., Boulanger, F., Desert, F. X. & Puget, J. L. 1999, A&A, 344, 322-332.

Lonsdale. C. J. 1995, in STSci Inst. Ser. 7, Extragalactic Background Radiation, ed. D. Calzetti, M. Livio, & P. Madau, (Cambridge Univ. Press) p. 145

Low, F. & Tucker, W. 1968, Phys. Rev. Lett., 21, 1538

Malkan, M. & Stecker, F. 1998, ApJ, 496, 13

Matsumoto, T., Akiba, M., Murakami, H. 1988, ApJ, 332, 575

McLean, I. *et al.* 1993, in Infrared Detectors and Instrumentation, ed. A. Fowler, (Bellingham:SPIE), 513

McDowell, J. 1986, MNRAS, 223, 763

Noda, M. *et al.* 1992, ApJ, 391, 45

Partridge, R. B. & Peebles, P. J. E. 1967, ApJ, 148, 377

Peebles, P. J. E. 1969, Phil Trans. Royal Soc. London, A, 264, 279

Pei, Y. C., Fall, M. S., Hauser, M.G. 1999, ApJ, 522, 604

Pozzetti, L., Madau, P., Zamorani, G., Ferguson, H. & Bruzual, G. 1998, MNRAS, 298, 1133

Rieke, G. & Lebofsky, M. 1985, ApJ, 288, 618

Schlegel, D., Finkbeiner, D. & Davis, M. 1998, ApJ, 500, 525

Stanev, T. & Franceschini, A. 1998, ApJ, 494, L159

Wainscoat, R. *et al.* 1992, ApJS, 83, 111

Wright, E. 1985, PASP, 97, 451

Wright, E. 1992, ApJ, 391, 34

Wright, E. 1997, BAAS, 29, 1354

Wright, E. 1998, ApJ, 496, 1

Table 1. Photometry of Stars in the Dark Spot with  $K < 9$  mag or  $L < 9$  mag

Name	$\alpha_{2000}$	$\delta_{2000}$	LIRC2	J60	K60	K	L
D48	$13^h02^m53.7^s$	$51^{\circ}02'21''$	7.31	6.69	6.02	6.06	5.83
C61	$12^h56^m31.5^s$	$51^{\circ}04'49''$	6.36	7.11	6.36	6.42	6.17
A96	$13^h03^m09.1^s$	$51^{\circ}42'28''$	6.83	7.19	6.55	6.65	6.48
C250	$12^h52^m21.4^s$	$50^{\circ}16'56''$	7.63	7.78	7.51	7.58	7.51
D240	$12^h59^m31.9^s$	$50^{\circ}21'47''$	8.39	8.89	8.22	8.22	7.67
B192	$12^h54^m45.0^s$	$51^{\circ}33'50''$	8.08	8.43	7.89	7.97	7.72
A207	$12^h58^m17.5^s$	$51^{\circ}16'28''$	8.11	8.82	8.04	8.13	7.72
B262	$12^h52^m47.8^s$	$51^{\circ}12'09''$	8.14	8.56	8.29	8.32	7.84
A210	$12^h58^m17.5^s$	$51^{\circ}16'28''$	9.25	8.84	...	7.42	7.87
D78	$12^h57^m30.5^s$	$50^{\circ}49'26''$	8.10	8.47	7.96	8.04	7.88
D74	$12^h56^m52.3^s$	$50^{\circ}48'05''$	7.72	8.45	7.86	7.94	7.89
A13	$13^h00^m00.2^s$	$52^{\circ}08'03''$	8.45	9.49	8.82	8.85	8.11
C199	$12^h50^m56.4^s$	$50^{\circ}29'56''$	8.02	8.75	8.41	8.48	8.32
A57	$13^h01^m21.1^s$	$51^{\circ}51'50''$	8.82	9.55	8.79	8.87	8.38
A107	$12^h59^m44.0^s$	$51^{\circ}42'11''$	8.84	9.94	...	8.66	8.42
B257	$12^h52^m25.8^s$	$51^{\circ}14'13''$	9.02	9.41	...	9.04	8.44
B254	$12^h51^m50.4^s$	$51^{\circ}16'29''$	8.59	8.83	8.52	8.52	8.46
A86	$13^h02^m56.6^s$	$51^{\circ}48'14''$	8.83	9.89	...	8.59	8.47
B267	$12^h54^m52.6^s$	$51^{\circ}13'04''$	9.16	9.92	...	9.74	8.50
C261	$12^h54^m24.7^s$	$50^{\circ}15'43''$	8.80	9.32	8.75	8.81	8.72
B50	$12^h56^m43.5^s$	$52^{\circ}03'08''$	8.62	8.92	8.62	8.62	8.78
A175	$13^h00^m40.4^s$	$51^{\circ}24'27''$	9.00	9.23	...	8.97	8.88
A117	$12^h57^m52.1^s$	$51^{\circ}37'56''$	9.14	9.71	...	9.21	8.90
C211	$12^h53^m28.5^s$	$50^{\circ}28'24''$	8.86	10.39	...	8.82	8.91
C49	$12^h52^m44.3^s$	$51^{\circ}03'23''$	8.87	10.37	...	9.02	8.93
D221	$13^h02^m37.7^s$	$50^{\circ}24'44''$	8.62	9.31	8.88	8.88	9.04
B91	$12^h51^m47.5^s$	$51^{\circ}51'15''$	8.28	8.44	8.16	8.19	9.07
D60	$13^h01^m03.8^s$	$50^{\circ}59'28''$	8.90	9.13	...	8.79	9.51

Table 2. Decomposition of the DIRBE Intensity

Component	$2.2 \mu\text{m}$ kJy sr $^{-1}$	$3.5 \mu\text{m}$ kJy sr $^{-1}$
Total	$137.5 \pm 0.3$	$105.3 \pm 0.3$
Zodi	$101.8 \pm 3.8$	$80.4 \pm 3.3$
ISM	...	$1.1 \pm 0.2$
Stars, $m < 9$ mag	$7.4 \pm 2.2$	$5.3 \pm 1.8$
Stars, $m > 9$ mag	$11.9 \pm 0.6$	$5.7 \pm 0.3$
CIRB	$16.4 \pm 4.4$	$12.8 \pm 3.8$

Table 3. Diffuse Cloud Parameters

Parameter	Value	Description
$p_1$	1.2346	radial density exponent
$p_2$	0.4246	radial temperature exponent
$p_3$	3.5785	vertical “scale height”
$p_4$	0.9450	vertical density exponent
$p_5$	-1.3559	$\ln(\sin i)$ at break
$p_6$	0.3838	$10\times$ cloud pole $x$ component
$p_7$	-0.0758	$10\times$ cloud pole $y$ component
$p_8$	-0.0195	$10\times$ cloud offset $x$ component
$p_9$	-0.0471	$10\times$ cloud offset $y$ component
$p_{10}$	0.6098	$10\times$ density contrast of Dermott ring
$p_{11}$	5.5405	$\ln(T_B)$ , band temperature at $R = 1$
$p_{12S}$	0.5722	scattering scale factor for bands
$p_{12T}$	1.3851	thermal scale factor for bands
$p_{13}$	0.3161	the “dimple” in Dermott’s ring
$p_{14}$	7.8852	vertical scale for Dermott’s ring
$p_{15}$	-0.0226	spherical term in vertical density
$p_{16}$	0.0289	$\sin^2 i$ term in vertical density
$p_{17}$	-0.0262	additional density at $ \sin i  \approx 0.5$
$p_{18}$	-0.1977	additional density at $ \sin i  \approx 0.25$
$p_{19}$	-0.0294	additional density at $ \sin i  \approx 0.17$
$p_{20J}$	-0.2616	phase function linear coefficient at $1.25 \mu\text{m}$
$p_{20K}$	-0.2865	phase function linear coefficient at $2.2 \mu\text{m}$
$p_{20L}$	-0.2634	phase function linear coefficient at $3.5 \mu\text{m}$
$p_{21J}$	0.6761	phase function quadratic coefficient at $1.25 \mu\text{m}$
$p_{21K}$	0.5318	phase function quadratic coefficient at $2.2 \mu\text{m}$
$p_{21L}$	0.3988	phase function quadratic coefficient at $3.5 \mu\text{m}$

Table 4. Scattering and Emission Efficiencies

Parameter	Value	Description
$p_{22}$	0.6647	$\sigma_1$ scaling
$p_{23}$	0.7762	$\sigma_2$ scaling
$p_{24}$	0.7499	$\sigma_3$ scaling
$p_{25}$	1.8247	$\kappa_3$ scaling
$p_{26}$	1.3150	$\kappa_4$ scaling
$p_{27}$	1.1088	$\kappa_5$ scaling
$p_{28}$	1.2525	$\kappa_6$ scaling
$p_{29}$	0.8657	$\kappa_7$ scaling
$p_{30}$	0.7547	$\kappa_8$ scaling
$p_{31}$	0.8147	$\kappa_9$ scaling
$p_{32}$	0.6130	$\kappa_{10}$ scaling

Table 5. IRAS Band Parameters

Parameter	Value	Description
$q_1$	1.7058	$10 \times (\sin i)_{max}$ for Band 1
$q_2$	0.1963	Band 1 normalization
$q_3$	0.2722	$10 \times (\sin i)_{max}$ for Band 2
$q_4$	0.2515	Band 2 normalization
$q_5$	0.1167	$10 \times$ band pole $x$ component
$q_6$	-0.2691	$10 \times$ band pole $y$ component
$q_7$	-0.9321	$10 \times$ band offset $x$ component
$q_8$	1.9164	$10 \times$ band offset $y$ component
$R_1$	3.14	Outer radius for Band 1
$R_2$	3.02	Outer radius for Band 2